Published in final edited form as:
Eur J Cancer. 2010 June ; 46(9): 1668–1678. doi:10.1016/j.ejca.2010.02.017.

A novel microtubule-modulating agent induces mitochondrially-driven caspase-dependent apoptosis via mitotic checkpoint activation in human prostate cancer cells

Ritu Aneja[1,*], **Tohru Miyagi**[2], **Prasanthi Karna**[1], **Tucker Ezell**[1], **Deep Shukla**[1], **Meenakshi Vij Gupta**[3], **Clayton Yates**[4], **SR Chinni**[5], **Haiyen Zhau**[6], **Leland W. K. Chung**[6], and **Harish C. Joshi**[7]

[1]Department of Biology, Georgia State University, Atlanta, GA-30303

[2]Department of Cancer Therapy and Urology, Kanazawa University, Japan

[3]West Georgia Hospital, La Grange, GA 30240

[4]Department of Biology and Center for Cancer Research, Tuskegee University, Tuskegee, AL-36088

[5]Department of Urology and Pathology, Wayne State University School of Medicine, Detroit, MI 48201

[6]Department of Medicine, Cedars-Sinai Medical Center, Los Angeles, CA-90048

[7]Department of Cell Biology, Emory University School of Medicine, Atlanta, GA-30322

Abstract

Hormone refractory prostate cancer, its skeletal metastasis and complications remain a therapeutic challenge. Here we show that treatment with (S)-3-((R)-9-bromo-4-methoxy-6-methyl-5,6,7,8-tetrahydro-[1,3]dioxolo[4,5-g]isoquinolin-5-yl)-6,7-dimethoxyiso-benzofuran-1(3H)-one (EM011), the brominated analog of a plant-derived non-toxic antitussive alkaloid, noscapine, achieved significant inhibition of hormone-refractory human prostate cancer implanted intratibially in the bone as shown by non-invasive, real-time bioluminescent imaging of tumor growth in nude mice. Mechanistically, *in vitro* data suggested that the anti-proliferative and pro-apoptotic effects of EM011 in human prostate cancer cell lines were through blockade of cell-cycle progression by impairing the formation of a bipolar spindle apparatus. The G2/M arrest was accompanied by activation of the mitotic checkpoint, a pre-requisite for induction of optimal apoptosis. Attenuation of mitotic checkpoint by siRNA duplexes led to a reduction in mitotic arrest and subsequent apoptosis. Our results further demonstrated participation of an intrinsic mitochondrially-mediated apoptotic pathway that ultimately triggered caspase-driven EM011-induced apoptosis. EM011 did not exert any detectable toxicity in normal tissues with frequently dividing cells such as the gut and bone marrow. Thus, these data warrant further evaluation of EM011 for the management of prostate cancer.

[*]Corresponding author: Ritu Aneja, Department of Biology, Georgia State University, Atlanta, GA-30303. raneja@gsu.edu.

Conflict of interest statement: None Declared

Introduction

Prostate cancer is the second leading cause of cancer death in men with African-Americans being 65% more likely to be diagnosed than Caucasian-Americans or Hispanic men (1,2). An overwhelming majority (~90%) of prostate cancer deaths occur in patients with skeletal metastases, particularly in bones (3). Despite improved diagnosis and early treatment (surgery and anti-androgen therapies), the successful therapy of prostate cancer remains a challenge (4,5). Androgen-deprivation is regarded as the optimum first-line chemotherapeutic treatment for recurrent prostate cancer for patients who progress to systemic disease, or less commonly for those who initially present with advanced disease (6,7). Unfortunately, androgen-ablative therapy is only palliative, as tumors almost inevitably become refractory to anti-androgens within 6 months to 2 years (8,9). Chemotherapy of this hormone-refractory disease thus has been an intense area of investigation over the last few decades. Although recent studies of docetaxel-based chemotherapy in men with androgen-independent prostate cancer have indicated survival benefits for the first time, serious systemic taxane toxicities such as peripheral neuropathy, gastrointestinal toxicity, and immunosuppression have been encountered owing to their non-selective action and overpolymerizing effects on microtubules (10-13). Nevertheless, these studies yield promising possibilities for targeting microtubules and in turn, tubulin, which composes the microtubules, as a viable strategy for the therapeutic development of agents for the management of hormone refractory prostate cancer (14).

Noscapinoids are an emerging class of microtubule-modulating anticancer agents based upon the founding molecule, noscapine. Noscapine, a naturally-occurring plant alkaloid with known antitussive function was recently discovered for its tubulin-binding anticancer property (15). Continued efforts directed towards rational drug-design have resulted in the synthesis of several more potent noscapine analogs with superior pharmacologic and toxicity profiles (16-24). Owing to their favorable non-toxic nature and unique mechanism of action, noscapine and its analogs have been extensively studied for their chemotherapeutic efficacy in several preclinical models by various laboratories all over the world (25-29). Recently, the parent molecule noscapine was shown to demonstrate effective antitumor activity in human non-small cell lung cancer xenograft models (30). The brominated noscapine, EM011, has been reported to have superior bioavailability and higher anticancer efficacy than the parent, while retaining the non-toxic attributes of the parent molecule, noscapine (17,18,21,31,32). Although we have previously reported the therapeutic effectiveness of EM011 in human breast and drug-resistant lymphoma xenograft models (17,18,21), we asked if other cancer types also responded to a similar extent upon EM011 treatment. Since prostate cancers represent a biologically complex heterogenous state, we wished to examine the potential usefulness of EM011 in the treatment of prostate cancer.

Employing a non-invasive bioluminescent assay of tumor measurement in real-time, we here show that EM011 inhibits intratibial xenografts of hormone-independent human prostate cancer in nude mice without any detectable toxicity. Essentially, EM011 halts cell-cycle progression by induction of an aberrant multipolar mitosis with an activated mitotic checkpoint characterized by recruitment of spindle-assembly checkpoint proteins such as BubR1 and Mad2. It appears that this activation of spindle-assembly checkpoint is necessary for the robust induction of apoptosis in prostate cancer cells. Apoptosis was characterized by a collapse of mitochondrial transmembrane potential and alteration of expression levels of Bcl2 family members followed by an activation of the executioner-caspase machinery. These data elucidate an intrinsic mitochondrially-driven, caspase-dependent mechanism of apoptotic cell death in hormone-independent PC-3 prostate cancer cells. In addition, induction of *in vivo* apoptosis as evident by TUNEL staining was perhaps responsible for tumor inhibition in response to EM011 treatment. Thus, these data suggest EM011 as an attractive chemotherapeutic strategy for the management of hormone refractory human prostate cancer.

Materials and Methods

Cell lines, reagents and chemicals

Hormone-independent human prostate cancer cell lines (C4-2, C4-2B, PC-3) and a hormone-sensitive line, LNCaP, were maintained in T-medium (Invitrogen, Carlsbad, CA) supplemented with 10% FBS. PrEC normal human prostate epithelial cells were obtained from Clonetics (San Diego, CA) and were maintained in the PrEGM medium (Clonetics). Luciferase-tagged PC-3 cells (PC-3-luc) were prepared by stably transfecting and selecting cells containing firefly luciferase cDNA under control of a CMV-promoter. The brominated analog of noscapine, EM011 was prepared as described previously (16,19). EM011 was dissolved in dimethylsulfoxide (DMSO, vehicle) and stored as 10 mM and 100 mM stock solutions at -20°C until use.

Mad2 and BubR1 siRNA

Mad2, BubR1, and luciferase siRNAs (21-nucleotide duplexes) were designed to target Mad2 sequence 50-ACCTTTACTCGAGTGCAGA-30, BubR1 sequence 50-CAATACTCTTCAGCAGCAG-30, and luciferase sequence 50-CGTACGCGGAATACTTCGA-30, respectively. The siRNAs were synthesized by Dharmacon and transfected in cells with Lipofectamine-2000 reagent following manufacturer's instruction.

In vitro cell proliferation assay

PC-3, LNCaP, C4-2 and C4-2B cells were seeded in 96-well formats and treated the next day with increasing concentrations (0.01 μM-1000 μM) of EM011. At 72 hr post-treatment, cells were fixed and stained with 0.4% sulforhodamine B (SRB), which measures cell density by binding to cellular proteins (33). Percentage of cell survival as a function of drug concentration was then plotted to determine the IC_{50} value (drug concentration needed to prevent cell proliferation by 50%).

Cell-cycle analysis and immunofluorescence microscopy

Cells were seeded in culture dishes and grown until 70% confluence. The medium was then replaced with new medium containing either vehicle (0.1% DMSO) or 25 μM EM011 for 24, 48 and 72 hrs. After the incubation period, cells were fixed in 70% ethanol overnight followed by staining with propidium iodide (PI) solution containing RNase A for 45 min in dark. Samples were then analyzed on a FACSCalibur flow-cytometer (Beckman Coulter Inc., Fullerton, CA). For confocal immunofluorescence microscopy, cells were grown on coverslips, drug-treated and processed as described earlier (16).

Determination of mitochondrial transmembrane potential

The ampholytic cationic fluorescent probe $DiOC_6(3)$ was used to monitor the EM011-induced changes in the mitochondrial transmembrane potential. Briefly, PC-3 cells were seeded at a density of 10^6 and treated for 0, 24, 48 and 72 hr with EM011. After drug treatment, cells were loaded with the probe $DiOC_6(3)$ (40 nM) for 30 min at 37°C followed by flow-cytometric analysis as described earlier (17).

Terminal deoxynucleotidyl-transferase-mediated dUTP nick-end labeling (TUNEL) assay for apoptosis

DNA strand breaks were identified using the TUNEL assay as described (17,21). PC-3 cells treated with 25 μM EM011 for 72 hr were washed with ice-cold PBS, fixed in 1% paraformaldehyde, and 3′-DNA ends were detected using APO-BrdU TUNEL Assay Kit (Molecular Probes, Eugene, OR).

Determination of caspase-3 activity

PC-3 cells were incubated with 25 μM EM011 for 0, 12, 24, 48 and 72 hr post-treatment. Caspase-3 activity was measured by the cleavage of the small synthetic substrate Z-DEVD-aminoluciferin (CaspaseGloTM 3/7 Assay Kit, Promega, Madison, WI) that becomes luminogenic upon cleavage. The luminescent signal, which is directly proportional to the amount of caspase-3 activity, was measured using a luminescence plate reader.

Xenograft model of human prostate cancer

5- to 6-week old male BALB/c nude mice were obtained from NCI (Frederick, MD, USA). For intratibial injections, mice were anesthetized using ketamine/xylazine/acepromazine, the knee was flexed, and a 28-gauge, 1/2-inch, needle was inserted into the proximal end of tibia and 10^6 PC-3-luc cells in 20 μl were injected directly into the tibial-marrow. Growth of inoculated cells in mouse tibia was monitored by measuring luciferase activity in live mice using the IVIS imaging system (Xenogen Corp., Alameda, CA, USA). Tumors were allowed to grow until they could be detected by the IVIS system, and then, mice were randomly separated into two groups of 10 mice each. The treatment group animals received 300 mg/kg body weight EM011 (dissolved in water, pH 4) daily by oral gavage. The control group animals were treated daily with same volume of vehicle solution. All animal experiments were performed in compliance with the institutional IACUC guidelines.

Mice imaging

In vivo bioluminescent imaging was conducted on a cryogenically cooled IVIS system using LiveImaging acquisition and analysis software (Xenogen Corp.). Briefly, mice were anesthetized with ketamine/xylazine/acepromazine and subsequently received an intraperitoneal injection of 25 mg/ml luciferin potassium salt (Xenogen Corp.) in PBS. The animals were then placed in a light-tight chamber and imaged with a cooled charge-coupled device camera. Images were acquired 15 min after luciferin administration. An integration time of 20 seconds with 4 binnings of 100 pixels was used for luminescence image acquisition. Signal intensity was quantified as the sum of all detected photon counts within the lesion.

Bone marrow collection

At the end-point of control and treatment groups (35 days post-treatment with vehicle and EM011, respectively), bone marrow was collected from the femurs of mice from the control and EM011 treated groups. Animals were euthanized by CO_2 asphyxiation and the skin and muscle tissue was removed from the hind limbs which were then disarticulated from the skeleton. The proximal and distal epiphysises of both femurs were removed, and the femur shafts were placed in 10% phosphate-buffered formalin. Decalcified specimens of bilateral femurs, were post-fixed in buffered 10% formalin, dehydrated, paraffin-embedded, stained with haematoxylin-eosin and examined with Olympus BX40 light microscope.

Histopathologic and immunohistochemical analyses

At the end-point of control and treatment groups (35 days post-treatment with vehicle and EM011, respectively), spleen, small intestines, colon, kidney, liver, brain, heart, and lung were formalin-fixed, paraffin-embedded and 5 μm sections were stained with haematoxylin-eosin. TUNEL staining of tumor tissue sections was performed as previously described (17,18).

Statistical analysis

The mean and SE were calculated for all quantitative experiments using Microsoft-Excel software. The Student's t test was used to determine statistically significant differences between groups. p values of ≤ 0.05 were considered statistically significant.

Results and Discussion

EM011 shows antiproliferative activity in human prostate cancer cells

EM011 has been shown to significantly inhibit proliferation of lymphoma and breast cancer cells including those that have become resistant to treatment with conventional chemotherapeutic drugs (18,20,21). To this end, we first asked if prostate cancer cells responded to the antiproliferative effects of EM011 treatment. To this end, a panel of prostate cancer cells with varying degree of metastatic characteristics and variable hormone-dependence were employed. Hormone-independent PC-3 cells, along with three additional cell types with varying metastatic potential, i.e., the parental androgen-responsive non-metastatic LNCaP and its lineage-derived, androgen-independent (C4-2) and bone-metastatic (C4-2B) cells were used in the study. Since different cell lines due to inherent genetic variability are susceptible to different concentrations of a given drug, IC_{50} of EM011 was determined in each cell type using the sulforhodamine B (SRB) assay. The analyses revealed the half-maximal growth inhibitory concentration of EM011 as 5.6, 7.7, 10 and 12 μM, for PC-3, LNCaP, C4-2 and C4-2B, respectively (Fig. 1A). In normal prostate epithelial cells, PrEC, EM011 showed an IC_{50} of >100 μM. This suggested selectivity of EM011 for prostate cancer cells compared to normal epithelial cells (Supplementary Fig. 1).

It was noteworthy to observe that PC-3 cells, which lack endogenous androgen receptor (AR) expression, were more sensitive to EM011 than LNCaP, C4-2, C4-2B cells, which express various forms of mutated AR and exhibit hypersensitivity to androgen stimulation (34). Recent reports indicate that the microtubule-binding drug, paclitaxel, failed to decrease AR activity in C4-2B cells compared to PC-3 cells (35). Thus, it is likely that the lack of AR expression in PC-3 cells is perhaps responsible for their increased sensitivity to EM011. Although further investigation of the effect of EM011 on AR is currently underway in our laboratory, our data show that EM011 exerts antiproliferative effect in diverse cellular models of prostate cancer. Furthermore, given the lack of available effective therapies for prostate cancer, our data support the usefulness of EM011 in androgen dependent and independent prostate cancer due to its significant antiproliferative effects.

EM011 impedes cell-cycle progression by causing a G2/M arrest

To next determine the precise cell-cycle stage at which the drug intervenes to cause cell death, fluorescence-activated cell-sorting (FACS) was employed to quantitatively analyze the cell-cycle profiles of all four prostate cancer cell lines in a treatment time-dependent manner (Fig. 1B). Quantitation of these data showed that drug-treated cells accumulate in the G2/M phase at 24 hr post-treatment (Fig. 1C). At 48 and 72 hr of treatment, this arrested population declined and there was an emergence of a hypodiploid (<2N) sub-G1 population suggesting extensive DNA fragmentation, indicative of apoptosis (Fig. 1C). The distribution of cell population in the various cell-cycle phases (G0/G1, S, G2/M and sub-G1) for all the four prostate cancer cell lines (PC-3, LNCaP, C4-2, C4-2B) upon 25 μM EM011 treatment for the noted time points (0, 24, 48 and 72 hr) is shown in Supplementary Table 1.

EM011 perturbs spindle architecture and induces an aberrant mitosis

EM011 binds tubulin with a higher affinity than the parent molecule, noscapine (16,19). Having identified that EM011 impedes cell-cycle progression of prostate cancer cells, we next examined the effect of EM011 on the spindle morphology of PC-3 cells using confocal immunofluorescence microscopy. Interestingly, EM011 caused no detectable alterations in the microtubule arrays or nuclear morphology of interphase cells. The LNCaP and LNCaP-derived androgen-independent lines (C4-2 and C4-2B) showed dendritic-like appendages (distinct neuronal appearance) during interphase. Reports indicate that C4-2 cells established by inoculation of LNCaP cells into castrated mice exhibit androgen independency (36). Androgen

withdrawal causes androgen-dependent prostate cancer cells to adopt a pronounced neuroendocrine (NE) phenotype, suggesting that androgen receptor (AR) represses an intrinsic NE transdifferentiation process in prostate cancer cells. However, in all cell lines, independent of their androgen-receptor status, there was an accumulation of mitotic cells in prometaphase (white arrowheads) that displayed multipolar spindles at 24 hr of drug-exposure (Fig. 2). At 48 hr of EM011 treatment, multinucleate cells (open arrowhead) were evident indicating failed cytokinesis (Fig. 2). Apoptotic bodies (white arrows) were also visible at 48 and 72 hr (Fig. 2). These microscopy data correlated with the cell-cycle data that showed sub-G1 population indicating presence of fragmented DNA at 48 and 72 hr post-treatment.

EM011-mediated mitotic arrest involves activation of mitotic checkpoint

To ensure the fidelity of chromosome segregation, the mitotic checkpoint monitors mictotubule-kinetochore attachment, as well as tension generated across sister kinetochores by a bipolar spindle, before anaphase onset (37,38). Since EM011 perturbed spindle architecture and arrested cell-cycle progression, we wanted to next examine if EM011-induced mitotic arrest was accompanied by activation of the mitotic checkpoint. Mad2 and BubR1 are integral components required for checkpoint function and preferentially localize to kinetochores of unattached chromosomes (37). To assess the integrity of the mitotic checkpoint, we visualized the expression of BubR1 using immunofluorescence microscopy (Fig. 3A). There was a significant increase in BubR1 staining in 24 hr EM011-arrested cells. However, BubR1 immunostaining was almost absent in vehicle-treated cells that showed only some weak non-specific staining (Fig. 3A). The expression levels of BubR1 were also confirmed using immunoblotting methods (Fig. 3B). Our results showed that there was an increase in BubR1 expression upon EM011 treatment over time suggesting that drug-treatment activated the spindle assembly checkpoint in PC-3 cells (Fig. 3B).

EM011 induces robust apoptosis in PC-3 cells

The execution of apoptosis is characterized by changes in cellular morphology, including membrane blebbing, disruption of cytoskeleton, hypercondensation, fragmentation of chromatin material, and formation of apoptotic bodies (39). Although cell-cycle studies showed an induction of sub-G1 population, EM011-induced apoptotic cell death in PC-3 cells was further confirmed using a flow-cytometry based TUNEL assay that reliably quantitates apoptosis by enumerating cells with fragmented DNA (Fig. 3C). The values presented on cytograms are the percentage of apoptotic cells (top) and normal cells (bottom) (Fig. 3C). There were ~45% TUNEL-positive cells at 48 hr which peaked to ~67% at 72 hr (Fig. 3C) compared to controls (~2%), suggesting extensive DNA cleavage in PC-3 cells.

EM011-induced apoptosis essentially requires activation of mitotic checkpoint

EM011 treatment triggered activation of spindle checkpoint in PC-3 cells as evidenced by increased BubR1 expression. This checkpoint activation was perhaps associated with a transient mitotic arrest as confirmed by immunofluorescence and flow-cytometric studies. To determine if activation of mitotic checkpoint was a pre-requisite for the induction of apoptosis, siRNA duplexes for both Mad2 and BubR1 were employed to knock-down the expression of Mad2 and BubR1 in PC-3 cells (Fig. 4A). Knock-down of the spindle checkpoint by Mad2 or BubR1 siRNAs attenuated the ability of EM011 (24 hr exposure) to arrest the cell-cycle at G2/M phase (See histogram overlays, Fig. 4B). These data suggested a critical role of the spindle checkpoint in mediating EM011-induced G2M arrest. There was a reduction in the MPM-2 positive population (indicative of mitotic cells) upon siRNA knockdown of checkpoint proteins indicating attenuation of the mitotic population (Fig. 4C). The number of mitotic cells upon a 24 hr EM011 exposure in control (luc-siRNA) was ~51%. However, in BubR1 and Mad2 siRNA transfected PC-3 cells, the MPM-2 positive population significantly decreased to ~28%

and ~26% respectively, upon a 24 hr drug exposure (Fig 4C). The mitotic population in BubR1 and Mad2 siRNA transfected PC-3 cells was lower than the control (luc-siRNA) treated cells at all time points (0, 24, 48 and 72 hr) studied (Fig. 4D). Since mitotic arrest preceded cell death, we next investigated if attenuation of mitotically-arrested population caused by knockdown of BubR1 and Mad2 affected apoptosis. Interestingly, our results suggested that Mad2 or BubR1 knockdown caused a significant reduction in sub-G1 population in luciferase (control), Mad2, or BubR1 siRNA transfected cells upon EM011 treatment for 72 hr (histogram overlays, Fig. 4E). Quantitation of apoptotic cells (percent sub-G1 population) in luciferase (control), Mad2, or BubR1 siRNA transfected cells treated with EM011 for 0, 24, 48 and 72 hr is shown in Fig. 4F. Together, these data highlighted the importance of spindle checkpoint activation as a critical determinant of EM011-induced apoptosis in prostate cancer cells.

EM011 induces a mitochondrially-driven intrinsic apoptotic pathway in PC-3 cells

EM011 dissipates mitochondrial transmembrane potential—Our next goal was to gain insights into the apoptotic mechanisms recruited in PC-3 cells upon EM011 treatment to induce cell death. A collapse of mitochondrial potential ($\Delta\Psi_m$) is an important event in the initiation and activation of apoptotic cascades. Both extrinsically and intrinsically triggered apoptotic mechanisms usually lower mitochondrial potential that is responsible for driving production of ATP (40). Alterations in proapoptotic/antiapoptotic balance at the mitochondrial membrane are usually reflected as perturbations of mitochondrial membrane integrity and transmembrane potential. Thus, dissipation of mitochondrial membrane potential upon EM011 treatment was next evaluated using a cationic ampholytic fluorescent dye, 3,3′-dihexyloxacarbocyanine iodide ($DiOC_6(3)$) in a flow-cytometric assay. While the control vehicle-treated cells showed a single peak, 25 μM EM011 treatment resulted in a loss of $\Delta\Psi_m$ as evidenced by the appearance of a new peak with a shift in fluorescence due to reduced $DiOC_6(3)$ uptake (Fig. 5A). A quantitative bar-graph depicting the increase in the number of depolarized cells is shown in Fig. 5B.

EM011 treatment alters the expression of Bcl2 family members—The member proteins of the Bcl2 family consist of proapoptotic and antiapoptotic regulators of apoptosis (41). The established role of each protein is to either protect or disrupt mitochondrial integrity, thereby activating or inhibiting release of downstream factors such as cytochrome *c* that leads to activation of caspase-3, the key executioner of apoptosis. Bcl2 is a crucial regulator of apoptosis that is overexpressed in many types of cancer and high Bcl2 levels are associated with resistance of tumor cells to apoptosis induction by multiple anticancer drugs (42). Phosphorylation of Bcl2 protein is induced on serine residues in tumor cells arrested by microtubule-targeting drugs (eg. paclitaxel, vincristine, nocodazole) and has been associated with the inactivation of its antiapoptotic function through an unknown mechanism (43). Since BAX and Bcl2 are important players of the Bcl2 family that determine induction of apoptosis, we examined the effect of EM011 treatment over time on the expression levels of pBcl2, total Bcl2 and BAX in PC-3 cells. Immunoblotting data showed that EM011 treatment increased pBcl2 as well as BAX expression over time of drug treatment (Fig. 5C). The total Bcl2 levels remained unaffected (Fig. 5C). Another Bcl2 member, PUMA binds to Bcl2 and Bcl-X_L and induces changes in mitochondrial membrane potential and caspase activation (43). It has also been reported that expression of PUMA leads to translocation of BAX from cytosol to mitochondria and formation of BAX multimers in the mitochondria (44). Our immunoblotting data showed that EM011 induced an increase of PUMA levels until 36 hr and there was a decline thereafter (Fig. 5C).

EM011 activates a caspase-dependent apoptosis—The drop in mitochondrial potential eventually leads to activation of terminal cysteine proteases such as caspase-3/7 that can be monitored by a luminogenic substrate. This assay showed a tight correlation of EM011

incubation time and caspase-3 activation (Fig. 5D). Since several drugs can kill cells by non-apoptotic phenomena such as by necrosis (45), that does not perhaps require caspases, it was necessary to show a direct link between caspase activation and cell death. To this end, PC-3 cells were co-treated with EM011 and Z-VAD-fmk, a pharmacological inhibitor of caspase activity. In contrast to 48 hr EM011-alone treated cells (red profile), co-treated cells (48 hr) showed accumulation of multinucleated polyploid cells (upto 8N DNA, green profile, Fig. 5E). Shown in purple are vehicle-treated cells with normal cell-cycle (Fig. 5E). Similarly, immunofluorescence confocal microscopy results also corroborated these data, in that the 48 hr co-treated cells showed accumulation of multipolar and multinucleated cells while cells treated with EM011 alone showed several apoptotic bodies indicating induction of apoptosis. In contrast, control vehicle-treated cells showed a predominance of interphase cells. The above described cell phenotypes (interphase, multipolar, multinucleate, apoptotic) are represented in Fig. 5F. Quantitative analyses were in concordance with confocal microscopy observations (Fig. 5G). Thus, these data suggested that EM011 induced caspase-dependent apoptosis in PC-3 cells. To confirm activation of apoptotic effector caspases, cleavage of poly(ADP-ribose) polymerase (PARP) from its 116 kDa pro-form to its 89 kDa active form, a caspase-3 dependent event, was monitored. Immunoblotting data showed a time-dependent increase in cleaved PARP, a reliable marker of apoptosis (Fig. 5C).

Although our data showed that EM011 has an IC_{50} of 5.6 μM in PC-3 cells, the drug induced apoptosis at a much higher dose (25 μM) than the IC_{50} values. This may perhaps be ascribed to the distinction between the ability of the drug to suppress cell proliferation (i.e., the rate of cell division) and induce apoptosis (increase programmed cell death). The molecular determinants of cell proliferation and apoptosis are cell type- and drug-dependent (46). In the context of EM011, the suppression of cell proliferation by 50% occurred at a much lower concentration range than induction of apoptosis. We did not observe optimal apoptosis at lower concentrations (5-10 μM) in PC-3 cells (data not shown). Further insights into the signaling cascades that set into action upon drug exposure and regulate cell proliferation and apoptosis will perhaps be critical to delineate the dose dependency of these two processes. However, we do not discount the possibility that the drug's action to be cytostatic (to reduce cell proliferation) or cytotoxic (to induce apoptosis) may also depend on the cell-cycle phase in which the drug acts and the cellular context.

EM011 causes inhibition of tumor growth in intratibial prostate cancer xenografts

We have earlier reported the effectiveness of EM011 in regressing human xenografts of lymphomas and breast cancers in nude mice models (17,18,21). Since prostate cancer is inherently tougher to treat because of its aggressive and invasive nature, we next examined if the anticancer activity of EM011 extended to the less-treatable prostate cancer. A previously developed PC-3 human hormone-independent prostate cancer cell line that stably expresses luciferase (PC-3-luc) was chosen since it enables visualization and monitoring of prostate cancer growth non-invasively in real-time (47). This optical imaging technique offered the ability to not only monitor and quantify tumor growth and metastases in real-time in the whole animal, but also follow responses to EM011 treatment in longitudinal studies using the same cohorts of mice (Fig. 6A). In vehicle-treated control animals, the tumors showed unrestricted progression (Fig. 6B). In contrast, oral treatment with EM011 at 300 mg/kg showed a time-dependent inhibition of tumors at 35 days (Fig. 6B), though significant regression was evident as early as 14 days post-treatment (Fig. 6B). Quantification revealed a ~69.5% reduction in tumor volume at a confidence level of $p<0.05$, (n=10, Fig. 6B) on day 35 compared to vehicle-treated controls. Thus, *in vivo* experiments suggested that EM011 was effective in inhibiting growth of PC-3 cells in the bone, perhaps by interfering with mechanisms that dictate cellular proliferation and apoptosis. The current study employs PC-3 cells, which in most systems

produce bone tumors that are predominantly osteolytic. The PC-3 model, however, does not include an element of osteoblastic activity.

To next determine if apoptosis was in fact responsible for *in vivo* tumor reduction, TUNEL-staining was performed on tibial-sections from mice on day 21 post-treatment. Correlating with the timing of maximal rate of tumor inhibition, numerous TUNEL-positive cells were evident in tibial marrows from EM011-treated mice (Fig. 6C). Vehicle-treated controls, however, showed occasional TUNEL-positive cells (Fig. 6C). Furthermore, there was a high expression of cleaved caspase-3 (Fig. 6C) in the remaining small regressed tumors from EM011-treatment group indicating induction of apoptosis.

EM011 does not cause any pathological abnormalities

Chemotherapeutically or radiotherapeutically treated prostate cancer patients usually suffer toxicities in many tissues, particularly, tissues with actively proliferating cells (13). Unlike currently-available tubulin-binding agents employed in prostate cancer chemotherapy, EM011 turns out to be a well-tolerated, orally-available drug with no apparent toxicity. There were no detectable differences in the histological appearance of tissues including spleen, small intestine, colon, kidney, liver, brain, heart, and lung from vehicle- and EM011- treated tumor-bearing mice (Supplementary Fig. 2). To determine whether EM011 treatment affected the proliferation of normal tissues with rapidly proliferating cells, colonic crypts from drug-treated and vehicle-treated mice were stained with Ki67, a marker for proliferative index. We found that colonic crypts from drug-treated mice and vehicle-treated controls showed comparable nuclear Ki67 staining (Supplementary Fig. 3). Additionally, Ki67 staining was also observed in the follicles of the native lymphoid aggregates of colonic mucosa, consistent with continuing lymphoid cell proliferation in these drug-treated mice (Supplementary Fig. 4). These data suggested that EM011 did not affect normal tissues with frequently proliferating cells. Furthermore, histological evaluation of bone marrow from EM011-treated mice showed no evidence of any toxicity upon 300 mg/kg drug treatment. Normocellular bone marrow, exhibiting trilineage progressive hematopoiesis was observed in drug-treated mice. In addition, there was no evidence of marrow hypoplasia, dyspoiesis, necrosis, or fibrosis in EM011-treated mice. (Supplementary Fig. 5). Another major concern of antimicrotubule therapy is neurotoxicity perhaps due to the extreme effect of these drugs on microtubular trafficking in neurons leading to impaired axonal transport and peripheral neuropathies. Recently, our laboratory has shown that EM011 does not exert any neurotoxicity compared to taxotere using electrophysiological, behavioral and pathological measures in mice models (32).

Although the present study showed that EM011 inhibits cellular proliferation, impedes cell-cycle progression by activating the mitotic checkpoint, induces a multipolar mitosis followed by mitochondrially-mediated caspase-dependent apoptosis, several intriguing questions remain to be investigated. It is indeed interesting that subtle modulation of the dynamics of cellular polymers, microtubules, without major alterations of the monomer/polymer ratio of tubulin (32,48), can lead to selective apoptosis of prostate cancer cells and can perhaps form the basis for reduction of tumor burden. Perhaps, cells of healthy tissues, due to built-in cell-cycle checkpoints, halt the cell-cycle upon sensing problems in microtubule dynamics (48). On the other hand, cancer cells although seem to detect errors and arrest transiently, the arrest is not durable due to mutational lesions in checkpoint genes. Furthermore, EM011 manipulates an aberrant multipolar mitosis, which does not culminate in normal cytokinesis; rather mitotically-arrested cells probably slip out of mitosis into multinucleate cells that were evident at about 36-48 hr of drug-treatment. It seems likely that these multinucleate cells initiate apoptosis or continue to cycle thus accumulating further DNA amounts before triggering apoptosis. Based upon these data, we conclude that EM011 is a safe orally-available

microtubule-interfering therapeutic agent that warrants further evaluation for prostate cancer treatment.

Supplementary Material

Refer to Web version on PubMed Central for supplementary material.

Acknowledgments

This work was supported by grants to RA from Department of Defense (PC073104) and NCI (1K99CA131489) and to HJ from NCI (R01 CA095317).

References

1. Williams H, Powell IJ. Epidemiology, pathology, and genetics of prostate cancer among African Americans compared with other ethnicities. Methods Mol Biol 2009;472:439–53. [PubMed: 19107447]
2. Ross LE, Uhler RJ. Age, race, and repeated prostate-specific antigen (PSA) test use in the National Health Interview Survey. Ethn Dis 2006;16:244–7. [PubMed: 16599378]
3. Loberg RD, Logothetis CJ, Keller ET, Pienta KJ. Pathogenesis and treatment of prostate cancer bone metastases: targeting the lethal phenotype. J Clin Oncol 2005;23:8232–41. [PubMed: 16278478]
4. O'Reilly T, McSheehy PM, Wenger F, Hattenberger M, Muller M, Vaxelaire J, Altmann KH, Wartmann M. Patupilone (epothilone B, EPO906) inhibits growth and metastasis of experimental prostate tumors in vivo. Prostate 2005;65:231–40. [PubMed: 15948135]
5. Sava T, Basso U, Porcaro A, Cetto GL. New standards in the chemotherapy of metastatic hormone-refractory prostate. Expert Rev Anticancer Ther 2005;5:53–62. [PubMed: 15757438]
6. Hsieh CL, Chung LW. New prospectives of prostate cancer gene therapy: molecular targets and animal models. Crit Rev Eukaryot Gene Expr 2001;11:77–120. [PubMed: 11693967]
7. Kish JA, Bukkapatnam R, Palazzo F. The treatment challenge of hormone-refractory prostate cancer. Cancer Control 2001;8:487–95. [PubMed: 11807418]
8. Carroll PR, Kantoff PW, Balk SP, et al. Overview consensus statement. Newer approaches to androgen deprivation therapy in prostate cancer. Urology 2002;60(Suppl):1. [PubMed: 12231036]
9. Chodak GW, Keane T, Klotz L. Critical evaluation of hormonal therapy for carcinoma of the prostate. Urology 2002;60:201. [PubMed: 12137810]
10. Petrylak DP. Docetaxel for the treatment of hormone-refractory prostate cancer. Rev Urol 2003;5 (Suppl 2):S14–21.
11. Mancuso A, Oudard S, Sternberg CN. Effective chemotherapy for hormone-refractory prostate cancer (HRPC): present status and perspectives with taxane-based treatments. Crit Rev Oncol Hematol 2007;61:176–85. [PubMed: 17074501]
12. Moore CN, George DJ. Update in the management of patients with hormone-refractory prostate cancer. Curr Opin Urol 2005;15:157–62. [PubMed: 15815191]
13. Rowinsky EK. The development and clinical utility of the taxane class of antimicrotubule chemotherapy agents. Annu Rev Med 1997;48:353–74. [PubMed: 9046968]
14. Bhandari MS, Petrylak DP, Hussain M. Clinical trials in metastatic prostate cancer – has there been real progress in the past decade? Eur J Cancer 2005;41:941–53. [PubMed: 15808960]
15. Ye K, Ke Y, Keshava N, Shanks J, Kapp JA, Tekmal RR, Petros J, Joshi HC. Opium alkaloid noscapine is an antitumor agent that arrests metaphase and induces apoptosis in dividing cells. Proc Natl Acad Sci U S A 1998;95:1601–6. [PubMed: 9465062]
16. Zhou J, Gupta K, Aggarwal S, Aneja R, Chandra R, Panda D, Joshi HC. Brominated derivatives of noscapine are potent microtubule-interfering agents that perturb mitosis and inhibit cell proliferation. Mol Pharmacol 2003;63:799–807. [PubMed: 12644580]
17. Aneja R, Zhou J, Zhou B, Chandra R, Joshi HC. Treatment of hormone-refractory breast cancer: apoptosis and regression of human tumors implanted in mice. Mol Cancer Ther 2006;5:2366–77. [PubMed: 16985071]

18. Aneja R, Zhou J, Vangapandu SN, Zhou B, Chandra R, Joshi HC. Drug-resistant T-lymphoid tumors undergo apoptosis selectively in response to an antimicrotubule agent, EM011. Blood 2006;107:2486–92. [PubMed: 16282340]
19. Aneja R, Vangapandu SN, Lopus M, Viswesarappa VG, Dhiman N, Verma A, Chandra R, Panda D, Joshi HC. Synthesis of microtubule-interfering halogenated noscapine analogs that perturb mitosis in cancer cells followed by cell death. Biochem Pharmacol 2006;72:415–26. [PubMed: 16780803]
20. Aneja R, Lopus M, Zhou J, Vangapandu SN, Ghaleb A, Yao J, Nettles JH, Zhou B, Gupta M, Panda D, Chandra R, Joshi HC. Rational design of the microtubule-targeting anti-breast cancer drug EM015. Cancer Res 2006;66:3782–91. [PubMed: 16585205]
21. Aneja R, Liu M, Yates C, Gao J, Dong X, Zhou B, Vangapandu SN, Zhou J, Joshi HC. Multidrug resistance-associated protein-overexpressing teniposide-resistant human lymphomas undergo apoptosis by a tubulin-binding agent. Cancer Res 2008;68:1495–503. [PubMed: 18316614]
22. Aneja R, Vangapandu SN, Lopus M, Chandra R, Panda D, Joshi HC. Development of a novel nitro-derivative of noscapine for the potential treatment of drug-resistant ovarian cancer and T-cell lymphoma. Mol Pharmacol 2006;69:1801–9. [PubMed: 16517755]
23. Zhou J, Liu M, Luthra R, Jones J, Aneja R, Chandra R, Tekmal RR, Joshi HC. EM012, a microtubule-interfering agent, inhibits the progression of multidrug-resistant human ovarian cancer both in cultured cells and in athymic nude mice. Cancer Chemother Pharmacol 2005;55:461–5. [PubMed: 15690203]
24. Karna P, Sharp SM, Yates C, Prakash S, Aneja R. EM011 activates a survivin-dependent apoptotic program in human non-small cell lung cancer cells. Mol Cancer 2009;8:93. [PubMed: 19878573]
25. Barken I, Geller J, Rogosnitzky M. Noscapine inhibits human prostate cancer progression and metastasis in a mouse model. Anticancer Res 2008;28:3701–4. [PubMed: 19189652]
26. Mahmoudian M, Rahimi-Moghaddam P. The anti-cancer activity of noscapine: a review. Recent Pat Anticancer Drug Discov 2009;4:92–7. [PubMed: 19149691]
27. Hiser L, Herrington B, Lobert S. Effect of noscapine and vincristine combination on demyelination and cell proliferation in vitro. Leuk Lymphoma 2008;49:1603–9. [PubMed: 18766974]
28. Heidari N, Goliaei B, Moghaddam PR, Rahbar-Roshandel N, Mahmoudian M. Apoptotic pathway induced by noscapine in human myelogenous leukemic cells. Anticancer Drugs 2007;18:1139–47. [PubMed: 17893514]
29. Newcomb EW, Lukyanov Y, Schnee T, Ali MA, Lan L, Zagzag D. Noscapine inhibits hypoxia-mediated HIF-1alpha expression andangiogenesis in vitro: a novel function for an old drug. Int J Oncol 2006;28:1121–30. [PubMed: 16596228]
30. Jackson T, Chougule MB, Ichite N, Patlolla RR, Singh M. Antitumor activity of noscapine in human non-small cell lung cancer xenograft model. Cancer Chemother Pharmacol 2008;63:117–26. [PubMed: 18338172]
31. Aneja R, Dhiman N, Idnani J, Awasthi A, Arora SK, Chandra R, Joshi HC. Preclinical pharmacokinetics and bioavailability of noscapine, a tubulin-binding anticancer agent. Cancer Chemother Pharmacol 2007;60:831–9. [PubMed: 17285314]
32. Aneja R, Asress S, Dhiman N, Awasthi A, Rida PC, Arora SK, Zhou J, Glass JD, Joshi HC. Non-toxic melanoma therapy by a novel tubulin-binding agent. Int J Cancer 2010;126:256–65. [PubMed: 19626589]
33. Skehan P, Storeng R, Scudiero D, Monks A, McMahon J, Vistica D, Warren JT, Bokesch H, Kenney S, Boyd MR. New colorimetric cytotoxicity assay for anticancer-drug screening. J Natl Cancer Inst 1990;82:1107–12. [PubMed: 2359136]
34. Zhou J, Geng G, Wu JH. Synthesis and in vitro characterization of ionone-based chalcones as novel antiandrogens effective against multiple clinically relevant androgen receptor mutants. Invest New Drugs. 2009 Apr 24; Epub ahead of print.
35. Gan L, Chen S, Wang Y, Watahiki A, Bohrer L, Sun Z, Wang Y, Huang H. Inhibition of the androgen receptor as a novel mechanism of taxol chemotherapy in prostate cancer. Cancer Res 2009;69:8386–94. [PubMed: 19826044]
36. Wu HC, Hsieh JT, Gleave ME, Brown NM, Pathak S, Chung LW. Derivation of androgen-independent human LNCaP prostatic cancer cell sublines: role of bone stromal cells. Int J Cancer 1994;57:406–12. [PubMed: 8169003]

37. Zhou J, Panda D, Landen JW, Wilson L, Joshi HC. Minor alteration of microtubule dynamics causes loss of tension across kinetochore pairs and activates the spindle checkpoint. J Biol Chem 2002;277:17200–8. [PubMed: 11864974]
38. Amon A. The spindle checkpoint. Curr Opin Genet Dev 1999;9:69–75. [PubMed: 10072359]
39. Elmore S. Apoptosis: a review of programmed cell death. Toxicol Pathol 2007;35:495–516. [PubMed: 17562483]
40. Fadeel B, Orrenius S. Apoptosis: a basic biological phenomenon with wide-ranging implications in human disease. J Intern Med 2005;258:479–517. [PubMed: 16313474]
41. Reed JC. Bcl-2 family proteins. Oncogene 1998 Dec 24;17(25):3225–36. [PubMed: 9916985]
42. Green DR, Reed JC. Mitochondria and apoptosis. Science 1998;281:1309–12. [PubMed: 9721092]
43. Pathan N, Aime-Sempe C, Kitada S, Basu A, Haldar S, Reed JC. Microtubule-targeting drugs induce bcl-2 phosphorylation and association with Pin1. Neoplasia 2001;3:550–9. [PubMed: 11774038]
44. Yu J, Zhang L, Hwang PM, Kinzler KW, Vogelstein B. PUMA induces the rapid apoptosis of colorectal cancer cells. Mol Cell 2001;7:673–82. [PubMed: 11463391]
45. Jiang Q, Wong J, Ames BN. Gamma-tocopherol induces apoptosis in androgen-responsive LNCaP prostate cancer cells via caspase-dependent and independent mechanisms. Ann NY Acad Sci 2004;1031:399–400. [PubMed: 15753180]
46. Rixe O, Fojo T. Is cell death a critical end point for anticancer therapies or is cytostasis sufficient? Clin Cancer Res 2007;13:7280–7. [PubMed: 18094408]
47. Hsieh CL, Xie Z, Liu ZY, et al. A luciferase transgenic mouse model: visualization of prostate development and its androgen responsiveness in live animals. J Mol Endocrinol 2005;35:293–304. [PubMed: 16216910]
48. Landen JW, Lang R, McMahon SJ, Rusan NM, Yvon AM, Adams AW, Sorcinelli MD, Campbell R, Bonaccorsi P, Ansel JC, Archer DR, Wadsworth P, Armstrong CA, Joshi HC. Noscapine alters microtubule dynamics in living cells and inhibits the progression of melanoma. Cancer Res 2002;62:4109–14. [PubMed: 12124349]

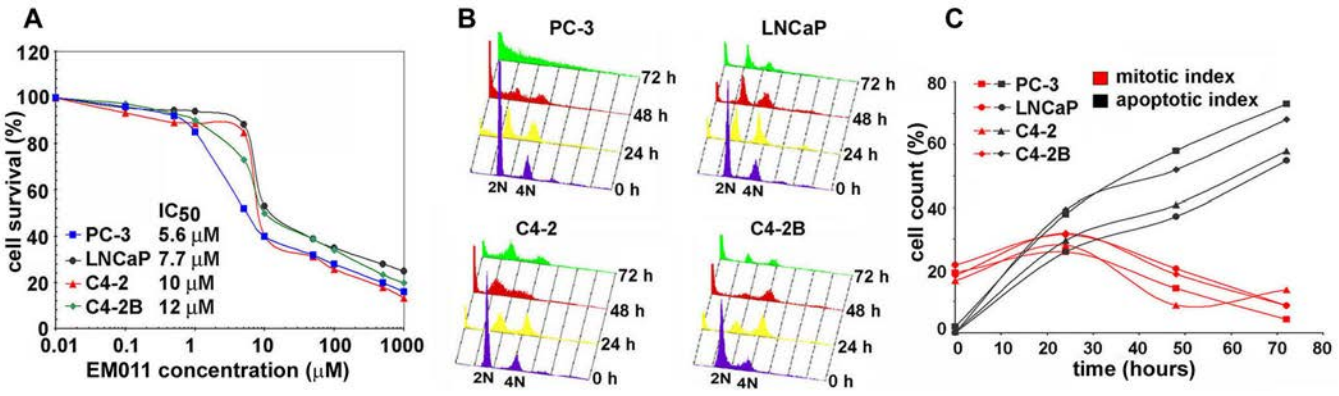

Figure 1.

EM011 inhibits cellular proliferation and impedes cell-cycle by causing mitotic arrest followed by apoptosis in PC-3, LNCaP, C4-2, and C4-2B cells. **A.** Plot of the percentage of cell survival versus EM011 concentrations used for the determination of IC_{50} values. Cells were treated with increasing gradient concentrations of EM011 for 72 hr, and the percentage of cell proliferation at the indicated drug concentrations, compared with vehicle-treated cells, was measured by the standard sulforhodamine B assay as described in Materials and Methods. The IC_{50} values of EM011 for all four prostate cancer cell types are indicated on the panel. **B**. The effect of EM011 on the cell-cycle profile of all four prostate cancer cells are shown in a three-dimensional disposition. Cells were harvested for analysis at the indicated times, stained with PI and analyzed by fluorescence-activated cell sorting (FACS) using Cell-Quest Software. The x axis shows the intensity of PI fluorescence, which is indicative of the total DNA content of cells in different cell-cycle phases. The y axis depicts the number of cells in each phase of the cell-cycle and the z axis indicates the time points (0, 24, 48, and 72 hr). Results are representative of three experiments done in triplicate. **C.** Quantitative representation of mitotic and apoptotic index as a function of time of treatment with 25 μM EM011.

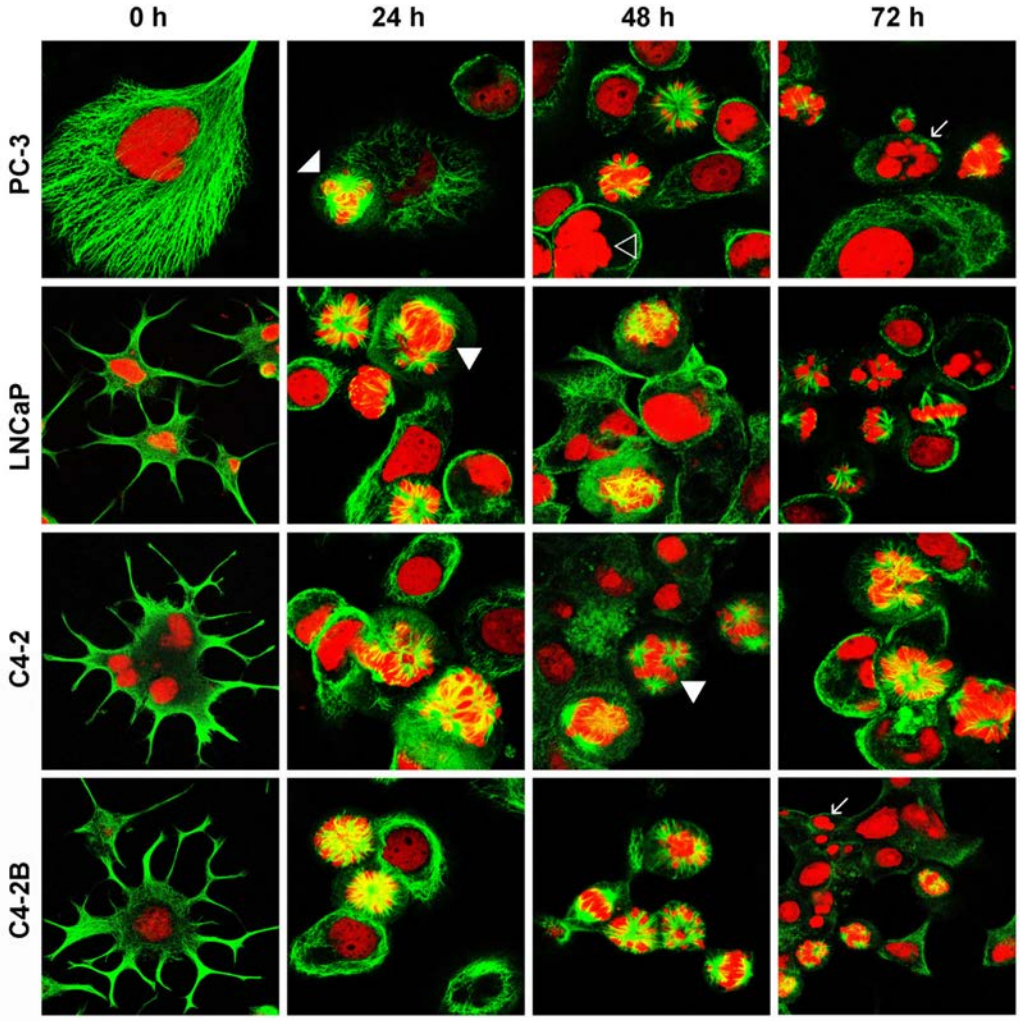

Figure 2.

EM011 perturbs spindle architecture and manipulates multipolar mitosis. Panel shows immunofluorescence confocal micrographs of prostate cancer cells stained for microtubules (green, FITC) and DNA (red, PI) upon 25 μM EM011 treatment for noted hours. There was an accumulation of mitotic cells in prometaphase (white arrowheads) with multipolar spindles at 24 hr of drug-exposure. At 48 hr of EM011 treatment, some multinucleate cells (open arrowhead) were evident and apoptotic bodies (white arrows) were visible at 48 and 72 hr.

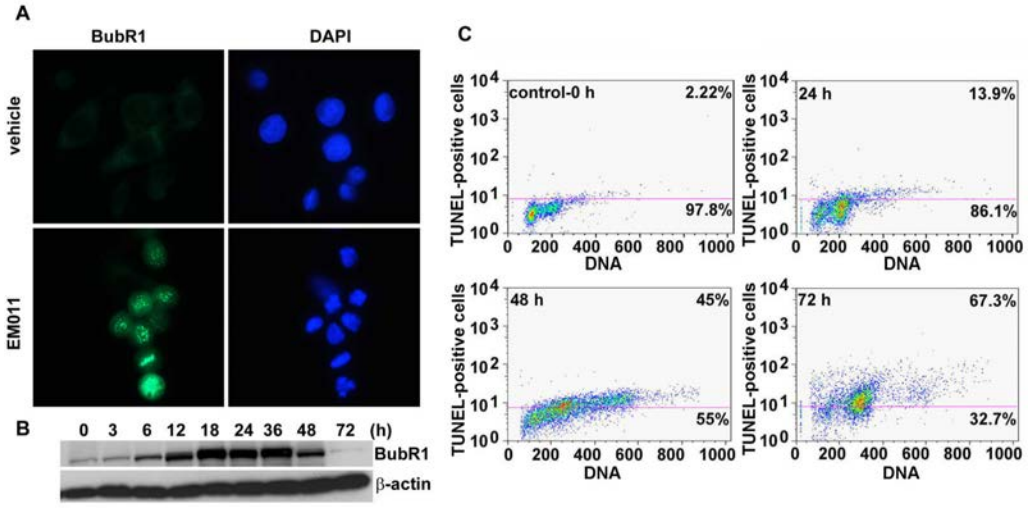

Figure 3.

EM011 induces activation of mitotic checkpoint. **A**. Mitotic arrest is mediated by spindle-assembly checkpoint, as visualized microscopically by immunofluorescent staining of BubR1 (green) at 24 hr post-treatment. **B**. Immunoblot analysis also showed BubR1 accumulation until 36 hr of drug treatment. β-actin was used as a loading control. **C**. EM011 treatment for 72 hr induces apoptosis in PC-3 cells. Fragmented DNA in the terminal apoptosis stages was quantified using terminal deoxynucleotidyl transferase–mediated bromo-dUTP reaction (TUNEL assay) in EM011-treated cells. After the indicated incubation periods, cells were processed for a flow cytometry-based terminal deoxynucleotidyl transferase-mediated BrdUTP reaction. The addition of BrdUTP to the terminal deoxynucleotidyl transferase reaction labels DNA strand breaks that are then detected by an Alexa-Fluor 488-labeled anti-bromodeoxyuridine antibody. DNA content was determined using propidium iodide (PI, x axis). The number of apoptotic cells is indicated by the number of Alexa-Fluor 488-positive cells (vales on the top of the cytogram). Data from a representative experiment of two experiments.

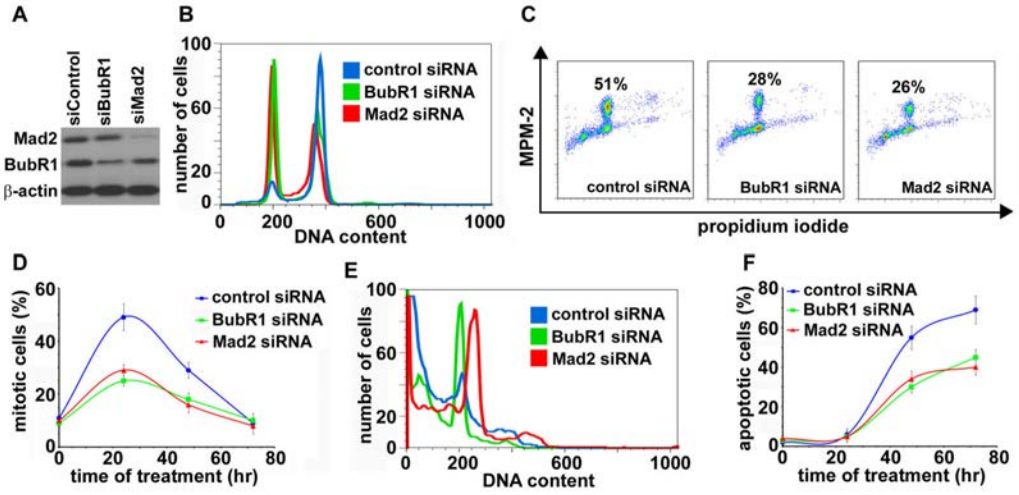

Figure 4.

EM011-induced apoptosis requires activation of spindle assembly checkpoint. Impairment of the spindle checkpoint by knock-down of Mad2 or BubR1 expression by specific siRNAs suppresses EM011-induced mitotic arrest and apoptosis. **A.** Immunoblot analysis of Mad2 and BubR1 expression in PC-3 cells transfected with luciferase (control), Mad2, or BubR1 siRNAs for 24 hr. Cells transfected with Mad2, BubR1, or control siRNAs for 24 hr were treated with 25 μM EM011 for 0, 24, 48, or 72 hr. **B.** Histogram-overlays of cell-cycle profiles of 24 hr drug-treated PC-3 cells that were transfected with luciferase (control), Mad2, or BubR1 siRNAs. **C.** Mitotic cells quantified by a mitosis-specific MPM-2 antibody in 24 hr drug-treated cells (transfected with luciferase (control), Mad2, or BubR1 siRNAs) using dual-color flow cytometry. **D.** Quantitation of MPM-2 positive cells in luciferase (control), BubR1 or Mad2 siRNAs transfected cells that were treated with EM011 for 0, 24, 48 and 72 hr. Values represent averages and error bars show SD ($p < 0.05$). **E.** Histogram-overlays of cell-cycle profiles of luciferase (control), BubR1 or Mad2 siRNA transfected cells that were drug-treated for 72 hr depicting differences in sub-G1 population (indicative of apoptotic cells). **F.** Quantitation of apoptotic cells (sub-G1) shows that cells with attenuated checkpoint molecules had reduced apoptotic responses at the noted hours (0, 24, 48 and 72) upon drug-treatment. Values represent averages and error bars show SD ($p < 0.05$).

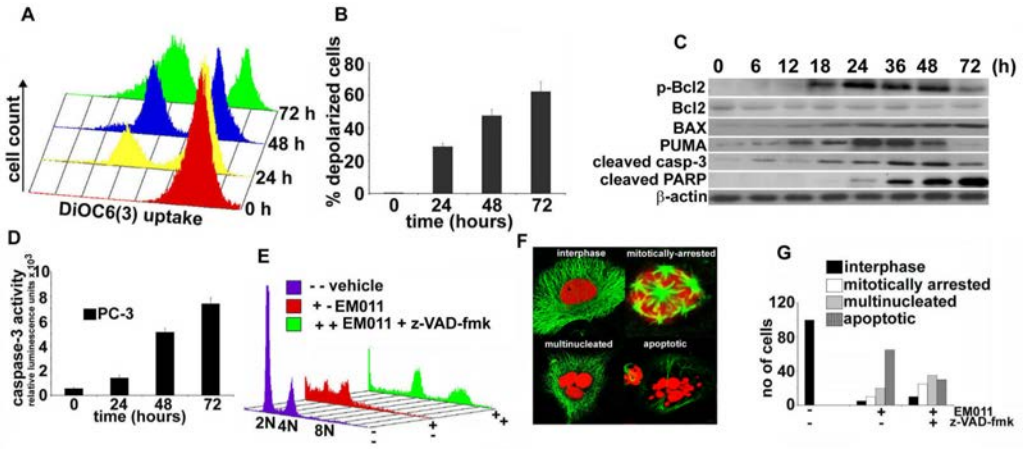

Figure 5.

EM011 treatment induces a mitochondrial-driven caspase-dependent apoptosis. **A.** Mitochondrial potential drop is observed beginning 24 hr of 25 μM EM011 exposure that progressively peaks at 72 hr as revealed by FACS-analyses using fluorescent-marker, DiOC6 (3). **B.** Quantitation of time-dependent increase in the number of depolarized cells upon 25 μM EM011 treatment. Values represent averages and error bars show SD ($p < 0.05$). **C**. Immunoblot analyses for p-Bcl2, total Bcl2, BAX, PUMA, activated caspase-3 and cleaved PARP over time of EM011 treatment. **D**. In the same time-frame, significant activation of caspase-3 activity also occurs as measured luminogenically. **E.** Caspase-inhibitor, z-VAD-fmk, along with EM011 treatment for 48 hr significantly reduces sub-G1 population while accumulating polyploid cells (green profiles). Cells treated with EM011 alone for 48 hr (red profiles) show significant apoptotic population as compared to vehicle-treated controls (purple profiles). **F.** Representative confocal immunomicrographs showing interphase, mitotically-arrested, multinucleated and apoptotic cells. Tubulin (*green*); DNA (*red*). These cell phenotypes were observed in different magnitudes upon treatment with drug alone or drug along with caspase inhibitor. The 48 hr co-treated cells show a larger proportion of cells with multipolar mitosis and multinucleation with excess DNA amounts. EM011-alone treated cells show preponderance of apoptotic bodies. **G**. Quantitation of these different cell phenotypes from random image fields totaling 100 cells in 48 hr PC-3 cells treated with vehicle, EM011, z-VAD-fmk, EM011+ z-VAD-fmk.

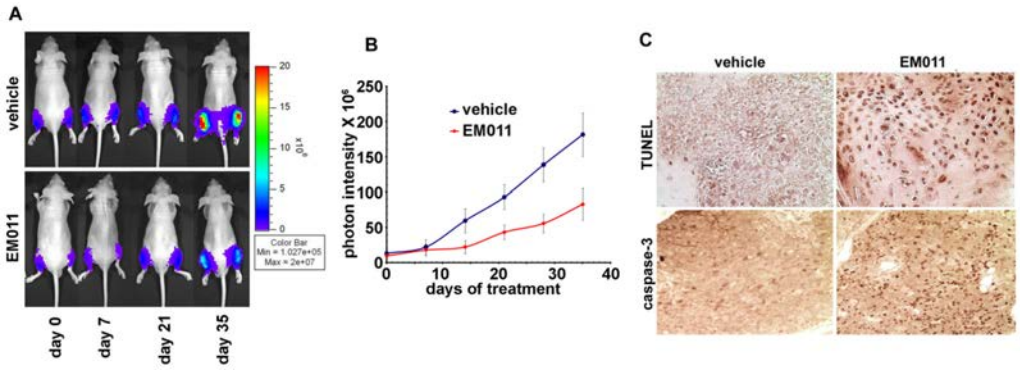

Figure 6.

Bioluminescent imaging shows tumor reduction of PC-3 intratibial xenografts upon EM011 treatment for five weeks. Cold (blue) colors indicate low photon counts whereas hot colors (red) show high counts. **A.** Top-panel shows representative mice and their tibial bioluminescence indicating progression of tumor growth in control vehicle-treated mice. Bottom-panel shows mice treated daily with 300 mg/kg EM011 by oral gavage. Note that a significant decrease of photon pixels was visible at day 35 of EM011 treatment. A steep upward transition of tumor growth occurs at day 21 in vehicle-treated mice. **B**. Quantitative evaluation of photon emission, thus, tumor burden. Stars represent significance at $p < 0.05$, n=10. **C**. Paraffin-embedded tibial-sections from vehicle-treated and 21 day EM011-treated mice were processed for TUNEL assay to visualize apoptotic cells. In contrast to controls, numerous TUNEL-positive cells were visible in EM011-treated sections. Significant cleaved caspase-3 immunostaining is also evident in sections from drug-treated mice compared to vehicle-treated controls.